Correcting for filter-based aerosol light absorption biases at ARM's SGP site using Photoacoustic data and Machine Learning

Joshin Kumar[1], Theo Paik[1], Nishit J. Shetty[1], Patrick Sheridan[2], Allison C. Aiken[3], Manvendra K. Dubey[3], and Rajan K. Chakrabarty[1]

[1]Center for Aerosol Science and Engineering, Department of Energy, Environmental and Chemical Engineering, Washington University in St. Louis, St. Louis, MO 63130, USA
[2]NOAA Global Monitoring Laboratory, Boulder, CO 80305, USA
[3]Earth and Environmental Sciences Division, Los Alamos National Laboratory, Los Alamos, NM 87545 USA

Correspondence to: Rajan K. Chakrabarty (chakrabarty@wustl.edu)

Abstract. Measurement of light absorption of solar radiation by aerosols is vital for assessing direct aerosol radiative forcing, which affects local and global climate. Low-cost and easy-to-operate filter-based instruments, such as the Particle Soot Absorption Photometer (PSAP) that collect aerosols on a filter and measure light attenuation through the filter are widely used to infer aerosol light absorption. However, filter-based absorption measurements are subject to artifacts ~~which~~ that are difficult to quantify. These artifacts are associated with the presence of the filter medium and the complex interactions between the filter fibers and accumulated aerosols. Various correction algorithms have been introduced to correct for the filter-based absorption coefficient measurements toward predicting the particle-phase absorption coefficient (B_{abs}). However, the inability of ~~Since previously developed correction~~ these algorithms to incorporate ~~might not undertake~~ in their formulations ~~all the~~ the complex matrix of influencing parameters such as ~~(~~ particle asymmetry parameter, particle size, and particle penetration depth~~, etc.) into account in their fixed analytical form,~~ ~~have a fixed analytical form, fundamentally, hence, they are unable to~~ results in prediction of ~~predict~~ ~~particle phase~~ particle-phase absorption coefficients with relatively ~~a the highest~~ low ~~degree of~~ accuracy. The analytical form of corrections also suffer from ~~a~~ lack of universal applicability ~~universally~~: different corrections are required for rural and urban sites across the world. In this study, we analyzed three months of high-resolution ambient data collected using a 3-wavelength photoacoustic spectrometer (PASS) and PSAP on the same inlet; both instruments were operated at the Department of Energy's Atmospheric Radiation Measurement (ARM) Southern Great Plains user facility in Oklahoma. We implemented the two most commonly used analytical correction algorithms, namely the Virkkula (2010) and the average of Virkkula (2010) and Ogren (2010)-Bond (1999), as well as a Random Forest Regression (RFR) machine learning algorithm to infer ~~particle phase~~ particle-phase B_{abs} values from PSAP data and estimate their accuracy in ~~comparsion~~ comparison to the reference B_{abs} values measured synchronously by the PASS. For the application on the SGP dataset, the RFR model was trained with an uncorrected absorption coefficient derived from PSAP ($B_{abs\ uncorrected\ PSAP}$), PSAP transmission ($Tr$), scattering coefficient from nephelometer (B_{scat}), and total mass concentration obtained from the sum of ACSM measured concentrations of various

1

species as input variables and particle-phase B_{abs} as the output variable. The wavelength averaged Root Mean Square Error (RMSE) values of B_{abs} predicted using the RFR algorithm are improved by an order of magnitude in comparison to those predicted by the Virkulla (2010) and average correction algorithms. A revised form of the Virkkula (2010) algorithm suitable for the SGP site has been proposed; however, its performance yields approximately two-fold errors when compared to the RFR algorithm. To further test the accuracy of our proposed RFR algorithm, we again trained and tested the model on a dataset of laboratory-generated combustion aerosols. The RFR model used as inputs the aerosol number size distribution from Scanning Mobility Particle Sizer (SMPS), uncorrected Tricolor Absorption Photometer (TAP)-derived B_{abs}, and nephelometer-measured scattering coefficient B_{scat} and predicted particle-phase B_{abs} values within 5% of the reference B_{abs} measured by a PASS. Machine learning approaches offer a promising path to correct for biases in long-term filter-based absorption datasets and accurately quantify their variability and trends needed for robust radiative forcing determination.

1 Introduction

Aerosols affect the climate through the absorption and scattering of radiation which has been the subject of intensive ongoing research (Brown et al., 2021). Aerosols are one of the most significant sources of uncertainty in climate model predictions of radiative forcing (IPCC, 2021). The U.S. Department of Energy's Atmospheric Radiation Measurement (ARM) program was established in 1990 to collect measurements to better understand processes that affect atmospheric radiation in climate models (Stokes and Schwartz, 1994). The ARM program currently operates three heavily instrumented fixed location sites to gather atmospheric data: Southern Great Plains (SGP), North Slope of Alaska (NSA), and Eastern North Atlantic (ENA). The SGP site is the world's most comprehensive climate research facility, with extensive *in situ* and remote sensing instrument clusters deployed over about 143,000 km^2 centered near Lamont, Oklahoma, USA. Instruments at the SGP site measure radiation, cloud properties, and other meteorological quantities (Sisterson et al., 2016). Light absorption data by aerosols at the SGP site is collected using Radiance Research's 3-wavelength Particle Soot Absorption Photometer (PSAP) (Sheridan et al., 2001) and DMT's 3-wavelength Photoacoustic Soot Spectrometer (PASS), an extension of the 1-wavelength instrument that was deployed at Jeju island, South Korea (Flowers et al., 2010) and in Utqiagvik, Alaska (Myers et al., 2021).

The PSAP instrument infers aerosol light absorption using a low-cost filter-based method by measuring transmittance through aerosol particles collected on a filter substrate. The instruments based on this method, such as PSAP, facilitate semi-continuous sampling of particles and produce time-averaged bulk absorption measurements (Pandey et al., 2016). Filter-based aerosol light absorption measurement instruments such as PSAP are widely used due to their low cost and operational ease, even though their accuracy suffers from "unquantifiable artifacts" such as multiple scattering, which can overestimate absorption(Bond et al., 1999; Clarke, 1982; Gorbunov et al., 2002), aerosol overloading on the filter which

2

can underestimate absorption (Arnott et al., 1999; Weingartner et al., 2003) and the changed morphology of the deposited

65 aerosol on the filter (Subramanian et al., 2007).

The PASS instrument was deployed at the SGP site ~~on~~ in January 2009, followed by its decommission in October 2015 with the goal ~~to evaluate~~of evaluating the PSAP biases by the ARM program. The PASS is a ~~first-principle~~ contact-free method to measure particle-phase aerosol light absorption coefficient (B_{abs}). The working principle of a PASS is described in detail in Arnott et al. (1999). Briefly, photons from a modulated laser beam are absorbed by light-absorbing aerosol particles. The

70 absorbed energy is transmitted as heat to the surrounding air, which results in ~~a~~ modulated pressure waves that are detected as sound waves by a microphone. The microphone can be calibrated to determine light absorption by the particles. The measurements from a PASS are highly accurate, but they have low sensitivity (1hr average signal/noise ratio ~0.2 Mm^{-1} at SGP), and ~~long term~~long-term deployments can be expensive. PASS also ~~have~~ has issues with liquid and/or multiphase particles, as some of the laser energy goes into the phase change associated with heating the particles rather than ~~the~~

75 producing acoustic waves.

Various correction algorithms (Bond et al., 1999; Virkkula et al., 2005; Li et al., 2020; Müller et al., 2014; Nakayama et al., 2010) based on a general analytical equation form, have been developed and used in climate research facilities across the world. The general form of the various previously developed correction algorithms for PSAP is summarised in Eqn. (2~~1~~), where f is some function that varies between different correction approaches and C_0 is a constant representing a fraction of

80 total light scattered by the particles collected on the filter. The absorption coefficient reported by PSAP (B_{abs_PSAP}) is auto-corrected using an empirical correction f(Tr) applied by the instrument firmware to correct for magnification of the aerosol absorption by the filter medium and nonlinearities in the response as the filter is loaded (Bond et al., 1999; Ogren et al., 2010). DOE's PSAP Instrument Handbook (Springston, 2018) reports the filter area (A_{PSAP}=17. 81mm^2) and parameters used for f(Tr) as shown in Eqn. (1). Therefore, to obtain the uncorrected absorption coefficients from PSAP, we undo the filter-

85 loading correction with the same parameters as mentioned in the Handbook.

$$B_{abs\_uncorrected\_PSAP} = \frac{A_{PSAP}}{Q_{PSAP}\Delta t} \ln\left(\frac{I(t)}{I(t+\Delta t)}\right) = \frac{B_{abs\_PSAP}}{f(Tr)} = \frac{B_{abs\_PSAP}}{\left(\frac{1}{1.317 \times Tr + 0.866}\right)} \tag{1}$$

$$B_{abs} = B_{abs\_uncorrected\_PSAP} \times f\big(Tr(\lambda), SSA(\lambda), AAE(\lambda)\big) - C_0(\lambda) \times B_{scat} \tag{2\text{1}}$$

90 These algorithms, however, are non-universal in applicability and hence limited in accuracy because the fitting parameters of the transmission functions calculated in such algorithms are based on datasets of laboratory-generated aerosols which may or may not represent the diverse aerosols types in various parts of the world (Collaud Coen et al., 2010; Zuidema et al., 2018). The large variation in results of correction creates a need for a universal systematic approach for correcting filter-based measurements that is more accurate than previously stated algorithms.

3

In this study, we used three months of high-resolution ambient data ~~measured~~ collected by the PASS and PSAP at ARM's SGP site; we corrected for filter-based absorption measurements using Virkkula (2010) (referenced as "unrevised Virkkula" going forward), Virkkula equation with revised coefficients for the SGP site (referenced as "revised Virkkula"), the average of unrevised Virkkula and Ogren (2010) modified Bond (1999) correction (referenced as "Average"), and the Random Forest Regression (RFR), which is a supervised ensemble Machine Learning (ML) algorithm used for a wide range of classification and regression predictive problems (Kumar and Sahu, 2021). We provide an inter-comparison of the performances of these algorithms on the sampled SGP data. ~~Our findings show that the revised and unrevised Virkkula (2010), as well as the Average algorithms need to be significantly revised to improve their accuracy. The RFR algorithm demonstrated a high degree of accuracy in predicting B_{abs} in comparison to the analytical correction forms discussed in this study.~~

2 Methodology

2.1 Ambient data from SGP observatory

This study used ambient ground-based aerosol data from the ARM user facility at SGP, Lamont, OK. Figure A1 provides the descriptive statistics of the raw data obtained from instruments and the optical parameters derived from it. Figure A2~~1~~ presents composition data collected by the Aerodyne's Aerosol Chemical Speciation Monitor (ACSM) instrument at the SGP site over the period of ~3 months from 27th Jun to 25th Sept~~,~~ 2015, which is the period of focus in this study. We observed that organics aerosols (OA) consist~~s~~ of more than 60% of the mass concentration followed by sulfphates, ammonium, ~~-~~and nitrate. The summary of BC concentration at the SGP site is shown in Fig. A3~~2~~, which presents the Field Campaign Data collected using the Sunset Model 4 Semi-Continuous OC-EC Instrument from 3rd June to 27th November~~,~~ 2013. The average Elemental Carbon (EC) and Organic Carbon (OC) concentrations were found to be 0.174 ± 0.123 and 2.267 ± 1.400 ug carbon/m^3 air, respectively. Figure A4~~3~~ illustrates the time series of the uncorrected aerosol absorption data as derived from ~~measured by~~ PSAP ($B_{abs\_uncorrected\_PSAP}$) and PASS (B_{abs}) ~~instruments~~. We observed that the average particle-phase B_{abs} at the SGP site ranged from 0 to 8 Mm^{-1} for most times with an average B_{abs} of 1.36 Mm^{-1} across all three wavelengths. A detailed description of the working of each of the instruments at the SGP site is present in their respective Handbooks published by the ARM and SGP AOS Instrument Handbook (J Uin et al., 2020). The overview of instruments as mentioned in their handbook is as follows - The PSAP's inlet was dried, and the air was sampled from the AOS high-flow aerosol inlet. Impactor with 1-um and 10-µm size cut-off is used in all AOS systems. The impactor alternates between the two sampling cutoffs (all particles < 1 µm and all particles < 10 µm). The flow split is mentioned to be 0.9 slpm for the instrument and 0.4 slpm for dilution flow. The PSAP has been operated by ARM (and many others in the global community) for almost 25 years with the same filter media, Pallflex E70-2075W, which is composed of quartz fibers on a cellulose backing. All published corrections factors were developed and measured using the Pallflex E70 media. The sample inlet air flowrate into the PASS's resonator was approximately 1 lpm. The external sample flow system is set to draw 7.5 lpm

4

through the Nephelometer. The ACSM handbook states the aerosol size range to be 40nm to 1um (vacuum aerodynamic diameter) and the sample entering the ACSM for analysis is pulled from the dry sample stream at 0.1 lpm controlled by a 100 µm critical orifice.

Previous studies have measured non-refractive submicrometer aerosol concentration and the composition of its organic and inorganic constituents at the SGP site (Parworth et al., 2015; Liu et al., 2021). Across all studies, the highest mass concentration at the SGP site occurs in the winter and decreases from spring to fall. The nitrates dominate during the winters, while OA accounting for more than 60% of total non-refractory particulate matter mass concentration dominates for the rest of the year. The B_{abs} and B_{scat} at 550 nm ranged from 0 to 10 Mm^{-1} and 0 to 50 Mm^{-1} from 2010 to 2013, respectively (Sherman et al., 2015). Also, since the site is rural, long-term transport aerosols (such as mineral dust, absorbing OA, and secondary organic aerosol – SOA) may affect local aerosol properties (Andrews et al., 2019).

In this study, high-resolution data from PASS, PSAP, nephelometer, and ACSM with sampling averaged intervals of 2sec, 1min, 1min, and 30min, respectively, were collected from 27 Jun to 25 Sept 2015 in the ARM user facility at SGP. The rationale behind choosing this short duration time frame was the availability of quality controlled PASS datasets; the High laser module corresponding to the Green Wavelength underwent an upgrade at the site in early 2015. From Figure A1(a), (d) and Figure A4, however, we suspect that either the newly installed 532nm PASS laser could be slightly overestimating absorption, or that the old 405nm and 781nm lasers could be slightly underestimating absorption compared to their true values. We preprocessed the data into the following three broad steps for each instrument; first, we only included those timestamps where data was valid across all instruments without incorrect (e.g. Negative absorption coefficients), suspect (e.g. PASS measurements > 15Mm^{-1} at the SGP site), and missing values (e.g. Missing timestamps corresponding to parallel instrument measurements). Second, we smoothed the data from all instruments into 1hr averages. Third, to compare the measurements from different instruments at the same wavelengths, we adjust the PASS-derived B_{abs} and nephelometer-derived B_{scat} to the PSAP's operating wavelengths. The absorption Ångström exponent (AAE) is an aerosol optical parameter used for aerosol characterization and to extrapolate a given particle-phase aerosol absorption coefficient to any wavelength of interest. The AAE and SAE values were inferred using Eqn. (3) and Eqn. (4) (Liu et al., 2018). Statistics of AAE and SAE values from SGP's PASS and nephelometer data are summarized in Figure A1. Since the standard deviations of AAE values for the SGP data were significantly high, time-dependent AAE and SAE values were used to extrapolate the particle phase absorption and scattering coefficients to the PSAP's operating wavelengths. The parameters B_{abs1} and B_{abs2} in the Eqn. (3) and (4) are the absorption coefficients at wavelengths λ_1 and λ_2.

$$AAE = -\frac{ln(B_{abs\,1}/B_{abs\,2})}{ln(\lambda_1/\lambda_2)} \tag{3}$$

$$SAE = -\frac{ln(B_{scat\,1}/\,B_{scat\,2})}{ln(\lambda_1/\,\lambda_2)} \tag{43}$$

160

The extrapolation of filter-based measurements to other wavelengths using AAE is less accurate than the extrapolation of PASS measurements because filter-based measurements are inherently biased due to artifacts and its extrapolation to other wavelengths further adds ~~too~~n error. In order to compare the measurements from different instruments at same wavelengths, the measured values from the particle-phase instruments - B_{abs} from PASS and B_{scat} from nephelometer, were extrapolated to

165 PSAP's operating wavelengths (467, 530, and 660 nm) using inferred AAE and SAE, respectively.
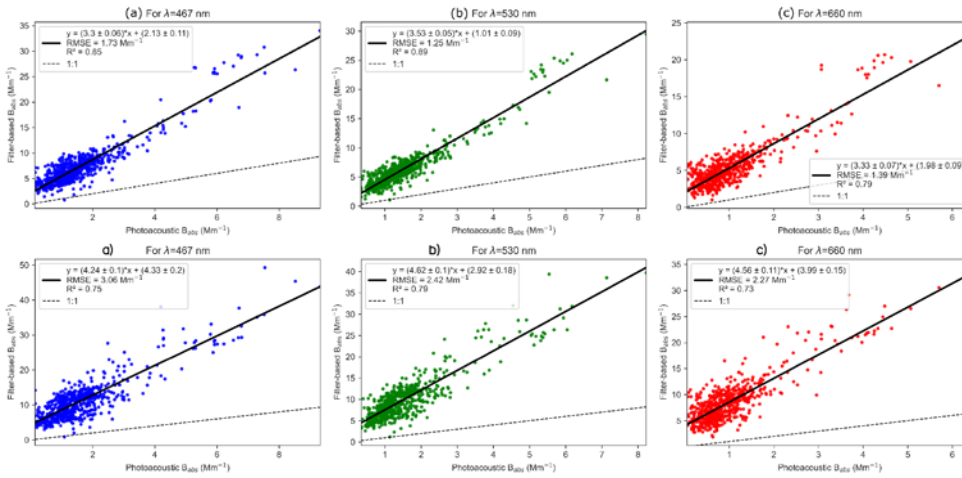
Figure 1: Scatterplot of absorption coefficients from the PSAP and extrapolated PASS measurements corresponding to (a) 467nm,
170 **(b) 530nm and (c) 660nm wavelengths at the SGP site.**

Figure 1 presents the comparison of uncorrected filter-based absorption coefficients ~~raw signals~~ with the calibrated, particle-phase ~~and accurate~~ B_{abs} measured using PASS. We observed that the uncorrected filter-based absorption coefficients ~~signals~~ are more than 4~~3~~ times greater than the ~~accurate~~ particle-phase B_{abs} measured by the PASS across all the wavelengths. Hence, at least for the SGP site, if we choose not to apply any correction algorithm ~~too~~n the filter-based absorption data, we

175 can use a factor of 4~~3~~ to obtain the B_{abs} with a wavelength-averaged RMSE (Root Mean Square Error) of 2.58~~1.45~~ ± 0.11~~0.2~~ Mm^{-1}. This overestimation of the filter-based aerosol light absorption measurements is due to the scattering of light away from the forward direction by the filter fibers ~~enhancement of light absorption by the filter deposited aerosol due to scattering based artifacts (Bond et al., 1999; Clarke, 1982; Gorbunov et al., 2002)~~ and due to the changed morphology of the deposited aerosol on the filter (Subramanian et al., 2007; Bond et al., 1999; Clarke, 1982; Gorbunov et al., 2002).

6

2.2 Correction algorithms

In order to correct for these "difficult-to-quantify" artifacts associated with the filter-based measurement of the aerosol absorption, various correction algorithms (Bond et al., 1999; Ogren, 2010; Virkkula et al., 2005; Li et al., 2020) have been introduced to predict the particle-phase absorption coefficient (B_{abs}) using filter-based absorption coefficient measurements. Ogren (2010) modified Bond (1999) and Virkkula (2010) correction algorithms are widely used in global atmosphere monitoring networks such as the Global Atmosphere Watch Programme (GAW) and the NOAA Federated Aerosol Network (Andrews et al., 2019). In this study, we only discuss the commonly used correction algorithms on the ground sites and compared them with the proposed ML-based filter correction algorithm.

2.2.1 Virkkula (2010) with unrevised parameters

Virkkula et al. (2005) developed an analytical correction equation that iteratively calculates B_{abs} from filter-based measurements. The transmittance correction function in the Virkkula equation was a multivariate function of the natural logarithm of transmission and SSA as shown in Eqn. (6). The parameters in the Virkkula equation h0, h1, k0, and k1 vary with wavelength. Virkkula (2010) recalculated these parameters by correcting for flowmeter calibration in Eqn. (6).

$$B_{abs} = B_{abs\_uncorrected\_PSAP} \times (k_0 + k_1 \ln(Tr)) \ - \ s \times B_{scat} \qquad (54)$$

$$B_{abs}(Virkkula\ corrected) = B_{abs\_uncorrected\_PSAP} \times (\ k_0 + k_1(h_0 + h_1\omega_0)\ ln(Tr)\ ) \ - \ s \times B_{scat} \qquad (65)$$

The parameters in Eqn. (4) and Eqn. (6) represent– particle phase absorption coefficient (B_{abs}), uncorrected absorption coefficient derived measurement from PSAP ($B_{abs\ uncorrected\ PSAP}$), transmission values from PSAP (Tr), particle phase scattering coefficient from Nephlometer (B_{scat}), single scattering albedo(SSA = ω_o = $B_{abs}/(B_{abs}+B_{scat})$) and Virkkula parameters/constants (k0, k1, h0, h1, s).

Using these parameters of the Virkkula equation, we calculated the B_{abs} values from the uncorrected filter-based absorption coefficients signals. Following the procedure mentioned in Virkkula (2005), dDue to the unknown values of SSA, the Virkkula equation was iteratively solved for the B_{abs}. The B_{abs} was first calculated using the Eqns. (54) and then was used to compute the initial guess for ω_o. Next, this value of ω_o was then used in Eqns. (6) to compute a more accurate value of B_{abs} and this procedure was repeated until B_{abs} value converged.

2.2.2 Virkkula (2010) with revised parameters for the SGP site

Using the reference measurements of B_{abs} from the PASS at the SGP site, we refitted the parameters in the Virkkula equation (h0, h1, k0, k1) to obtain revised parameters. The fitting was implemented using the "curvefit" function from the "SciPy" Python library, which uses non-linear least squares to fit a functional equation form to given data. After fitting of optimized parameters of the Virkkula equation, we solved for the particle phase absorption coefficients using the filter-based

7

absorption coefficients. It is important to note that the calculated revised Virkkula parameters may only be valid for the SGP site because these revised parameters were computed using the absorption data from PASS and PSAP at SGP site.

2.2.3 Ogren (2010)-Bond (1999) correction and its Average with~~of~~ unrevised Virkkula (2010) ~~and Ogren (2010)-Bond (1999)~~

215 Bond (1999) published a correction scheme for the PSAP which was updated by Ogren (2010). The Ogren (2010) modified Bond (1999) correction is applied using the Eqn. (7~~6~~) to obtain the corrected B_{abs} value. Another correction technique that is often used by the DOE ARM community involves computing a simple arithmetic mean of Virkkula (2010) correction with unrevised parameters and the Ogren (2010)-Bond (1999) correction to obtain a average corrected B_{abs} value as shown in Eqn. (8~~7~~) (C Flynn et al., 2020; Zuidema et al., 2018) For brevity, going forward we will refer to this correction scheme as the

220 "Average" correction algorithm.

$$B_{abs}(Bond~-/Ogren~corrected) = B_{PSAP} \times (\frac{1}{1.5557 \times Tr + 1.0227}) - 0.0164 \times B_{scat} \qquad (7\text{6})$$

$$B_{abs}(Average~corrected) = \frac{B_{abs}(unrevised~Virkkula~corrected) + B_{abs}(Bond/Ogren~corrected)}{2} \qquad (8\text{7})$$

225 **2.2.4 Random Forest Regression Model**

Random Forest Regression (RFR) is an ensemble supervised ML algorithm used for a wide range of classification and regression predictive problems (Kumar and Sahu, 2021). Random forest involves constructing a large number of decision trees with each decision tree fitted on a different subset of the training dataset (also called Bagging), in addition to selecting a random subset of input variables at each split point in the construction of trees. Random forest is known to reduce overfitting

230 of data in decision trees and provide accurate predictions (Biau, 2012; Breiman, 2001). The three most essential hyperparameters to tune the Random forest are: – 1. A number of random input variables to consider at each split point 2. The depth of the decision trees 3. The number of decision trees in the forest. The core concept behind the Random Forest is that it aggregates the results of many trained decision trees empirically and outputs the most optimal result.

ML algorithms perform very well on trained dataset; therefore, it is crucial to test their performance on unseen or untrained

235 data. We split the SGP dataset into training and testing sets in the ratio of 70:30. The training set was used to train the RFR model, and then the testing set was used to evaluate the model's performance on the new input data that the model had not encountered before. For the SGP data, w~~W~~e trained the RFR model with an uncorrected absorption coefficient derived from PSAP ($B_{abs~uncorrected~PSAP}$), PSAP transmission (Tr), scattering coefficient from nephelometer (B_{scat}), and total mass concentration obtained from the sum of ACSM measured concentrations of various species as input variables and particle-

240 phase B_{abs} as the output variable. ~~using the uncorrected B_{PSAP}, PSAP transmission, B_{scat}, and total mass concentration from ACSM as input variables and particle phase B_{abs} as the output variable.~~ The values of the hyperparameters used for the

8

construction of the RFR model are: the number of features to consider while looking for the best split = 5, the number of trees = 100, and the max_depth was such that nodes were expanded until all leaves were pure or until all leaves contain less than two samples.

245 The RFR algorithm is entirely a data-driven approach to correct filter-based measurements. The algorithm was trained on input-output variables, which were measured by different instruments installed at the site. The instrument detection limits, precision, and accuracy play a significant role in the training and predicting ability of the RFR algorithm. In order to gain highly accurate predictions from the RFR algorithm on the test dataset (data that is not used while training but is used to check the accuracy of the algorithm on unseen data), the algorithm requires good quality training data and with reasonably

250 large number of samples/instances in the training dataset to ensure that the algorithm's accuracy on the unseen test dataset is not limited by the number of samples of the training dataset on which it is trained upon. Figure A54 presents the general workflow of ML based correction models developed in this study.

255

3 Results

3.1 Application of Virkkula (2010) algorithm with unrevised parameters

	k_0	k_1	h_0	h_1	s
467 nm	0.377 ± 0.013	-0.640 ± 0.007	1.16 ± 0.005	-0.63 ± 0.09	0.015
530 nm	0.358 ± 0.011	-0.640 ± 0.007	1.17 ± 0.003	-0.71 ± 0.05	0.017
660 nm	0.352 ± 0.013	-0.674 ± 0.006	1.14 ± 0.11	-0.72 ± 0.16	0.022

Table 1: Unrevised parameters as mentioned in Virkkula (2010) to be used in Virkkula algorithm (i.e., Eqn. (65)).
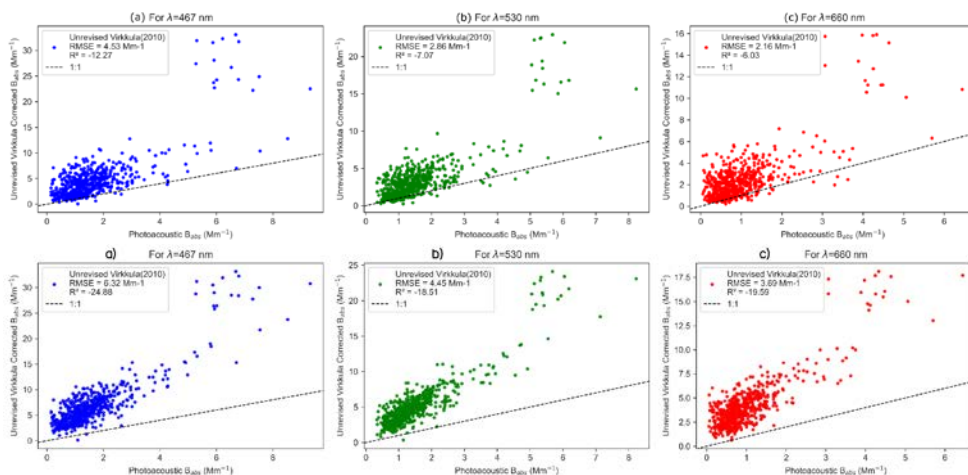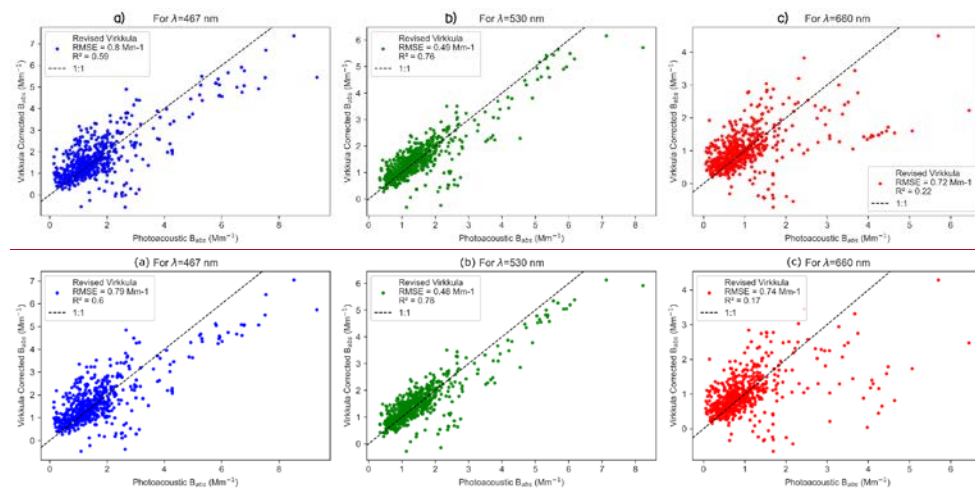
260

Formatted: Caption

Figure 2: Comparison between PSAP absorption coefficients, corrected for using Virkkula (2010) algorithm with unrevised coefficients, and the reference PASS absorption coefficients measured at the SGP site corresponding to (a) 467nm, (b) 530nm and (c) 660nm wavelengths.

The parameters mentioned in the Virkkula (2010) as shown in Table 1 were directly used to iteratively solve for B_{abs} using Eqn. (65). Figure 2 shows comparisons between the unrevised Virkkula calculated B_{abs} and reference B_{abs} measured using PASS. We observed that the %RMSE values (*calculated over all three wavelengths as = Σ_i (RMSE$_i$ / Mean Reference B$_{abs\_i}$) $\times$ 100*) which represents percentage of uncertainty for unrevised Virkkula in the calculation or predictions of B_{abs} is ~376240% and R^2 values are negative for all three wavelengths, which suggests that the unrevised Virkkula algorithm performs worse than a constant prediction of mean B_{abs} value.

The variance in B_{abs} calculated using unrevised Virkkula is large enough to undermine the algorithm's applicability without revising the parameters/coefficients. Since fitting parameters in Virkkula (2010) were based on experimental burn data of kerosene soot and "white" ammonium sulphate aerosol, those parameters cannot be universally applied to different types of ambient aerosols (Collaud Coen et al., 2010; Zuidema et al., 2018).

3.2 Application of Virkkula (2010) algorithm with revised parameters for the SGP site

	k$_0$		k$_1$	h$_0$		h$_1$		s
467 nm	0.141292	±	-0.0911 ± 0.0078	112.043998	±	-1015.3694	±	0.015
	0.0078			30.226045		31.33019		
530 nm	0.162344	±	-0.09203 ± 0.0067	0.04331.644	±	0.547-31.835	±	0.017

	0.0056			290.667318		2.7793.819		
660 nm	0.148311	±	-0.06427 ± 0.0057	-260.3065	±	-2063.30594	±	0.022
	0.0046			28.509782		29.6103		

Table 2: Revised parameters for the Virkkula equation computed using SGP dataset

Figure 3: Comparison between PSAP absorption coefficients, corrected for using the Virkkula algorithm with revised coefficients, and the reference PASS absorption coefficients measured at the SGP site corresponding to (a) 467nm, (b) 530nm and (c) 660nm wavelengths.

To overcome the imprecision of the unrevised Virkkula algorithm, we fitted the Virkkula equation to the SGP data to obtain revised Virkkula parameters (i.e., k0, k1, h0, h1) shown in Table 2. The same values of s were used as mentioned in Virkkula (2010) because parameter "s" represents a fraction of total light scattered which is experimentally determined by fitting to ammonium sulphate experiments (Virkkula et al., 2005). The Virkkula equation with these newly computed parameters was then used to iteratively solve for the B_{abs} using Eqn. (65). Figure 3 presents a comparison of filter-based absorption corrected using the revised Virkkula algorithm and reference B_{abs} measured using the PASS. We observed that the Virkkula algorithm performed comparatively well with revised parameters because the RMSE values decreased and R^2 values increased in comparison to unrevised Virkkula's evaluation metrics (i.e., RMSE, %RMSE and R^2). The results of Fig. 2 and Fig. 3 clearly imply that it is essential to revise the parameters before implementing the Virkkula equation for predicting B_{abs} at each site. Since the Virkkula equation does not undertake the seasonal, source and particle size distribution as inputs, the Virkkula parameters are subject to change with these external factors too.

11

295 It is important to note that since the B_{abs} predictions of revised Virkkula as shown in Fig. 3 were based on the same data that was used to calculate the Virkkula parameters, The performance of this algorithm on this data is the best that is possible. The %RMSE for the revised Virkkula predictions for the SGP data was ~58~7% which is less than that of unrevised Virkkula, but it still represents significant uncertainty in the calculation/prediction of B_{abs}. This major shortcoming of analytical fits led us to the ML approach to predict the B_{abs} using filter-based measurements.

3.3 Application of Ogren (2010) modified Bond (1999) correction and its aaverage withof unrevised Virkkula (2010) and Ogren (2010) modified Bond (1999)
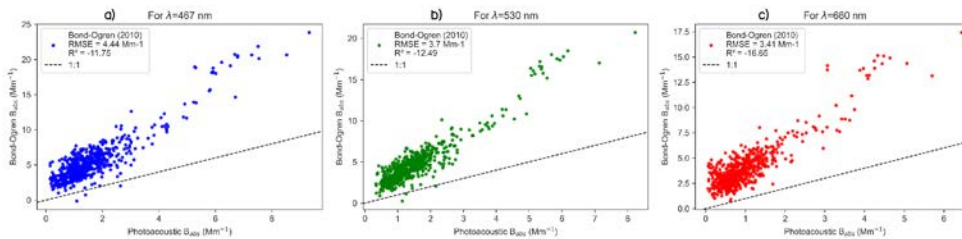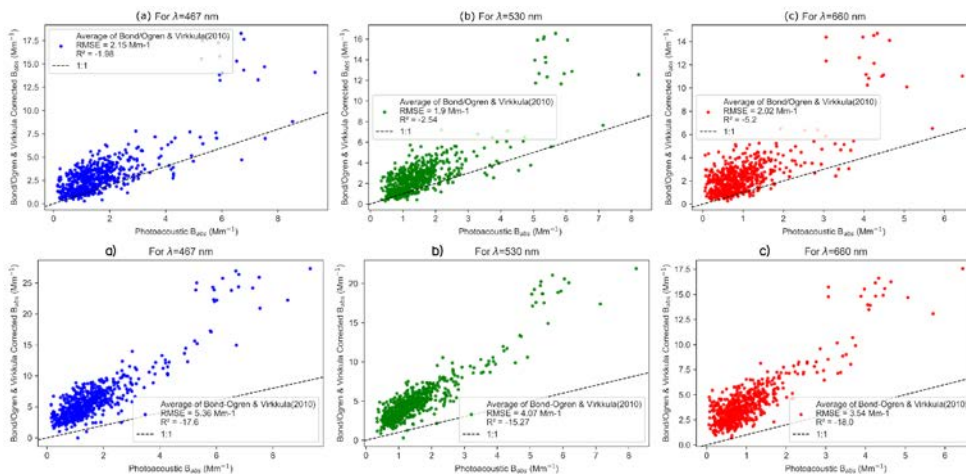

Figure 4: Comparison between PSAP absorption coefficients, corrected for using Bond-Ogren correction algorithm, and the reference PASS absorption coefficients measured at the SGP site corresponding to (a) 467nm, (b) 530nm and (c) 660nm wavelengths.

Figure 4 presents a comparison of filter-based absorption corrected using only the Ogren (2010) modified Bond (1999) algorithm as presented in Eqn. (7), and reference B_{abs} measured using the PASS. The %RMSE for this algorithm on the SGP data is ~312% which is almost the same as the %RMSE of unrevised Virkkula (2010). Since the general equation form of Ogren (2010) modified Bond (1999) is similar to that of Virkkula (2010) and both the unrevised versions of algorithms perform with similar accuracy, hence, the improvement in accuracy of Ogren (2010) modified Bond (1999) with revised coefficients can be expected to be very similar to that in the case of Virkkula.

Figure 54: Comparison between PSAP absorption coefficients, corrected for using the average of Bond- /Ogren and unrevised Virkkula (2010) algorithms, and the reference PASS absorption coefficients measured at the SGP site corresponding to (a) 467nm, (b) 530nm and (c) 660nm wavelengths.

Figure 54 presents a comparison of filter-based absorption corrected using the average of unrevised Virkkula (2010) and Ogren (2010) modified Bond (1999), and reference B_{abs} measured using the PASS. The %RMSE values for the "Average" correction are ~343170% and R^2 are negative for all three wavelengths suggesting that the model performs worse than a constant prediction of mean B_{abs} value. We observed that the "Average" correction performed better than the unrevised Virkkula but still worse than revised Virkkula algorithm. This justifies the application of "Average" algorithm at ARM sites for better accuracy when PASS-derived B_{abs} values are not available to revise the parameters of Virkkula equation and using just unrevised Virkkula algorithm yields low accuracy.

3.4 Application of Random Forest Regression (RFR) algorithm
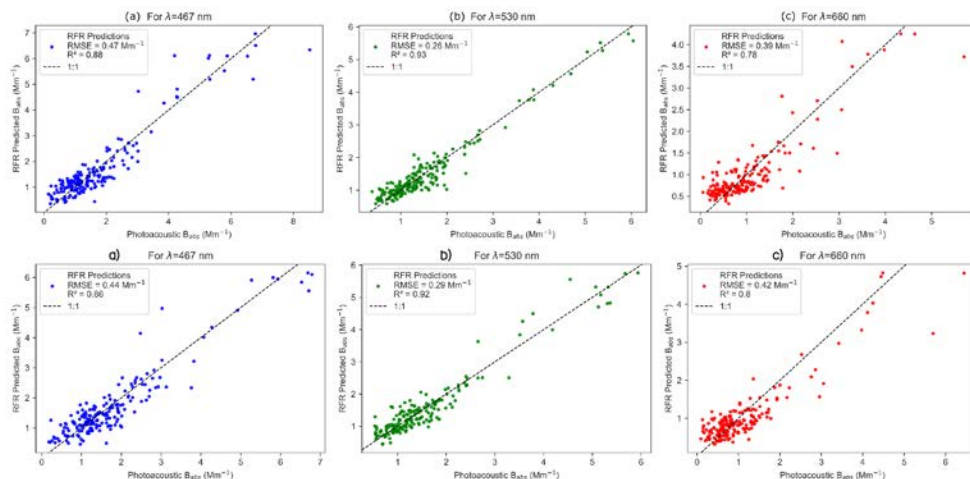
Figure 65: Random Forest Regression, a supervised machine learning algorithm, applied to correct for PSAP absorption coefficients, and comparison of its performance with reference PASS absorption coefficients measured at the SGP site corresponding to (a) 467nm, (b) 530nm and (c) 660nm wavelengths.

We used RFR, which is a supervised ML algorithm, to correct for the filter–based PSAP–derived uncorrected absorption coefficients ($B_{abs\ uncorrected\ PSAP}$) measurements. Figure 65 presents the comparison of RFR predicted B_{abs} with the reference B_{abs} measured using PASS. We observed from Fig. 65 that for all three wavelengths, %RMSE values for the B_{abs} predictions from the RFR algorithm are ~320%, and the R^2 values are also greater than ~0.8, which are much better than the evaluation metrics for both unrevised and revised Virkkula algorithms even when the RFR algorithm's evaluation metrics were computed on unseen test data.

Apart from the two common correction algorithms (Ogren (2010) modified Bond (1999) and Virkkula (2010)) applied to PSAP, recent attempts were made to develop new correction algorithms (Li et al., 2020) by constructing a multivariate linear model in the general correction Eqn. (21) and including the interaction terms between AAE, SSA, and ln(Tr). It was referred as "Algorithm A" by Hanyang et al. and produced the R^2 values of 0.62, 0.55, and 0.43 on the PSAP's operating wavelengths of 467nm, 528nm, and 652nm, respectively. Comparing just R^2 values, the RFR algorithm fares better than "Algorithm A" which is the most recent PSAP correction algorithm developed yet.

The RFR algorithm performs better than the analytical models because it empirically captures the nonlinearities and complex relationships between the input variables and B_{abs}, and it was trained on an extra input of total mass concentration from ACSM. It is important to note that after the eliminative pre-processing of the three months of bulk data, the number of valid

14

data samples that remained was relatively small for a typical ML algorithm training; we can expect that the RFR algorithm can perform even better with more extensive data.

3.5 Improving the accuracy of the Random Forest Regression (RFR) algorithm

RFR is an ensemble supervised machine learning algorithm which builds many decision ~~tress~~ trees using the input data
350 during the training phase and predicts the output as the mean of predictions from all of the trees. The accuracy of the RFR directly depends on the number of different or uncorrelated trees built during the training as shown in Fig. 76. In order to produce many uncorrelated trees, we not only train the trees on different random subsets of training data (i.e., Bagging) but also choose differerent input features or variables randomly to split the nodes. Training the RFR algorithm on all the input variables which significantly affect the output variable not only enables us to increase the number of uncorrelated trees built
355 during training but also constrains the model for accurate prediction. Hence, the accuracy of RFR to predict particle phase B_{abs} could be further improved by training the algorithm using all possible input variables that affect B_{abs}, such as $B_{abs\_uncorrected\_PSAP/TAP}$ from PSAP/TAP, transmission, B_{scat}, aerosol number size distribution parameters, and composition.
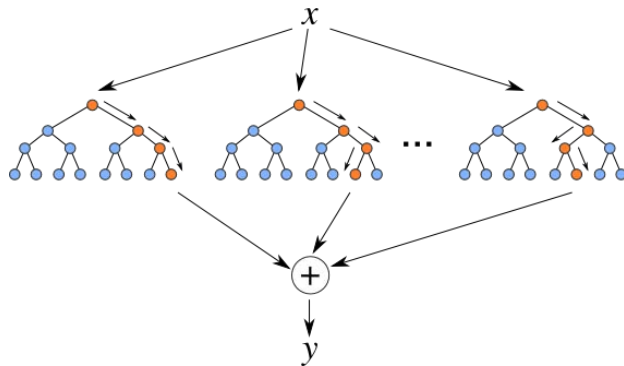

Figure 76: Flowchart of RFR illustrating many uncorrelated trees build using random feature sampling whose average prediction
360 **is more accurate than ~~the~~ each of the individual trees. (Adapted from Gitconnected)**

As a proof of concept, we trained and tested the RFR algorithm on a laboratory-generated published dataset of burn chamber experiments (Sumlin et al., 2018; Shetty et al., 2019; Shetty et al., 2021). The algorithm was trained using the total number concentration, geometric mean diameter, geometric standard deviation, uncorrected filter-based Tricolor Absorption Photometer (TAP) B_{abs}, and nephelometer B_{scat} as input variables, while the output variable was the particle-phase absorption
365 coefficient. Figure 87 presents the comparison of RFR predicted B_{abs} with the reference B_{abs} measured using PASS during the burn. We observed from Fig. 87 that the RFR algorithm correctly predicted the particle-phase B_{abs} within 5% (=%RMSE) of the reference B_{abs}. We also note that the R^2 values are ~1, which shows that the predictions correlate near-perfectly with

15

the reference PASS-derived absorption values. This example demonstrates the capabilities of RFR in capturing the complex relationship between filter-based measurements and particle-phase B_{abs} with the best possible accuracy.
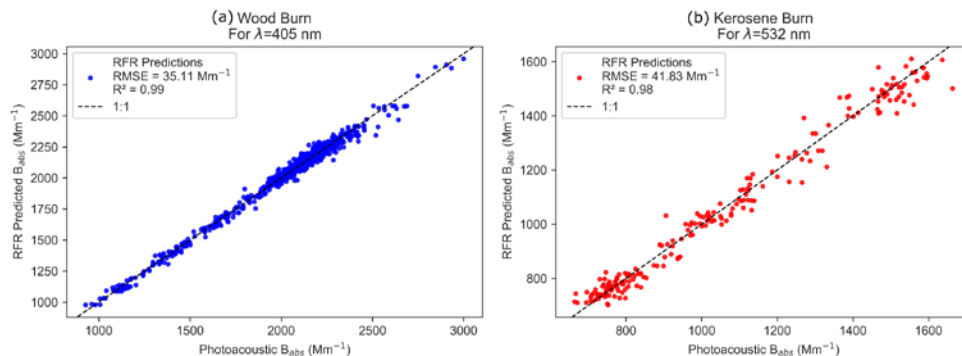
370

Figure 87: An illustration of the power of Random Forest Regression (RFR) algorithm in accurately predicting particle-phase absorption coefficient when trained with a robust set of input variables. The plots show the accuracy of RFR trained TAP absorption coefficients in comparison to the reference PASS absorption coefficients corresponding to (a) 405nm and (b) 532nm for laboratory-generated aerosols from combustion combu.

4 Conclusions

375

The uncertainties in predicting particle-phase absorption coefficients from filter-based absorption data are due to both measurement uncertainties of the instruments and the uncertainties of parameter computation while using analytical algorithms like those put forth in Virkkula (2010). Little can be done about the instruments' measurement uncertainties, originating from noise and calibration of instruments, STP correction, and flow rate uncertainties (Sherman et al., 2015).

380 However, using ML techniques, we can avoid the uncertainties introduced from by parameter computation and stiff functional forms, which are inevitable when using algorithms with analytical forms.

Our findings show that the revised and unrevised Virkkula (2010), as well as the Average algorithms, need to be significantly revised to improve their accuracy. We demonstrate that our RFR algorithm corrects for the PSAP filter–based biases in refernce reference to the PASS measurements at the SGP accurately and much better than the standard Virkkula

385 algorithm. A unique feature of the SGP site is that while there are significant monthly variations in the aerosol composition, the optical properties such as the B_{abs}, B_{scat}, and SSA are bounded in a small range with weak annual cycles. Because of this feature of the SGP site, we argue that the ML-based correction algorithm trained in this study is scalable to other months. Furthermore, the developed correction algorithm can be applied to any climate research facility site globally, provided the seasonality information is included as an input feature to the algorithm during the training using Label Encoding method

390 which can be used to convert categorical variable such as name of the months into numerical variable.

16

RFR was a ML algorithm of choice in this study because of its high accuracy even with relatively small training datasets (Kumar and Sahu, 2021). However, if training of a large dataset is involved, other techniques such as XGBoost and neural networks could improve accuracy further than RFR. The RFR algorithm captures nonlinear dependence between variables with the highest accuracy compared to the functional analytical form correction algorithms that were previously developed.

395   We confidently propose that ML models can produce the most accurate and fastest predictions possible of the particle phase absorption coefficients compared to any other analytical equation form algorithms, given the training data is accurate and of reasonable size.

Major aerosol monitoring networks, such as the Interagency Monitoring of PROtected Visual Environments (IMPROVE) network and the Chemical Speciation Network (CSN) collect particle samples for measurement of UV-VIS-IR absorption

400   coefficient. Correction scheme developed as part of this study might be applicable to infer aerosol light absorption properties for samples collected from the IMPROVE network, rural facilities and federal Class I areas. ML approaches offers promising path to correct long term of airborne filter based absorption observations to accurately quantify their variability and trends for robust climate radiative forcing determination. Future work will be in the direction of fine tuning the RFR algorithm to accurately predicting light absorption by biomass burning aerosols from the wildfires.

405

17

Appendix A

	Mean ± Std.
AAE (405-532)	-0.132 ± 2.480
AAE (532-781)	-2.432 ± 2.189
AAE (405-781)	-1.366 ± 1.579
SAE (450-550)	-1.522 ± 0.418
SAE (550-700)	-1.781 ± 0.448
SAE (450-700)	-1.663 ± 0.427
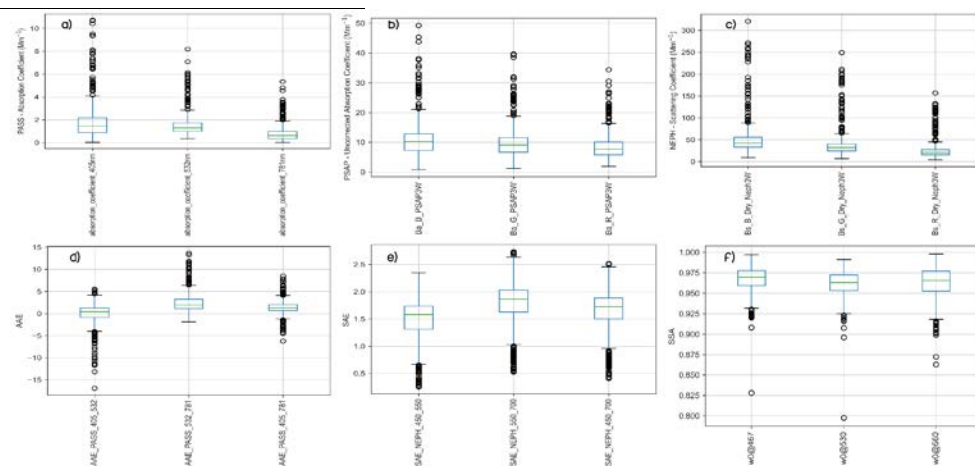
Figure A1: Summary of the SGP dataset. The boxplots of raw measurement data are shown as obtained from various instruments used in this study (a) PASS (b) PSAP{ $B_{abs\ uncorrected\ PSAP}$ } and (c) Nephelometer. The boxplots of parameters dervied from the raw data are also shown (d) AAE (e) SAE and (f) SSA. The green line is the median of the data. The bottom line of box is 25% percentile of data and top line of box is 75% percentile of data, therefore, the box represents the middle 50% of all the datapoints which is the core of the data.Table A1: Mean and standard deviation of AAE and SAE values calculated for the SGP data.
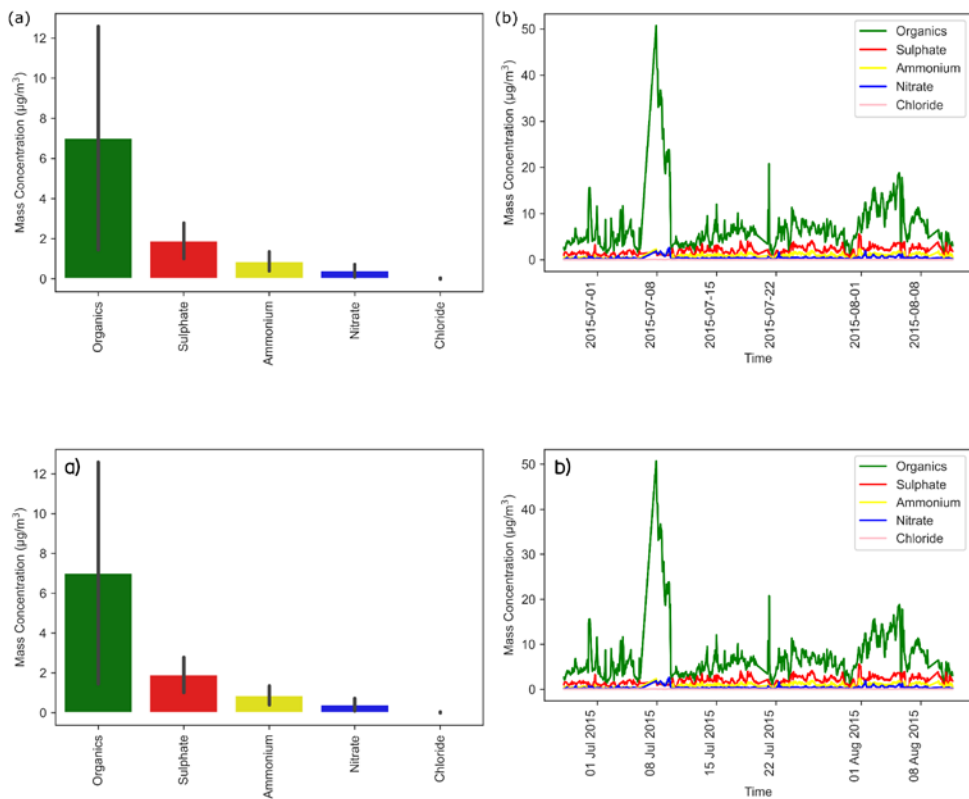
Figure A21: Composition of the ambient ground measurement site at SGP. The error bars represent the standard deviations. (a) Mass concentrations of various species (b) Timeseries of the absolute mass concentration of particle chemical composition.
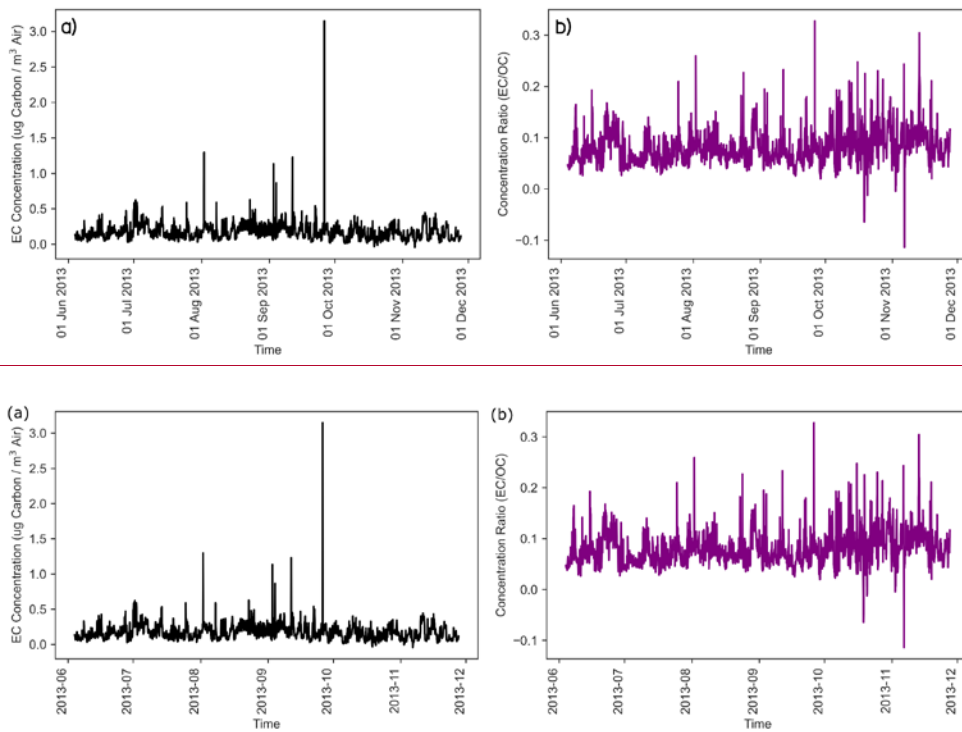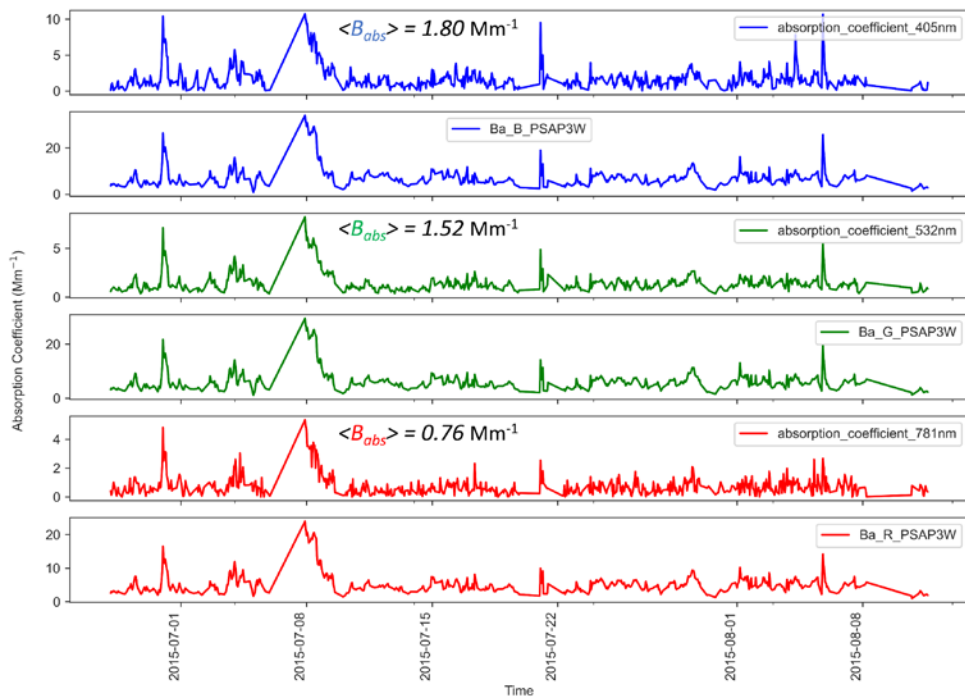
Figure A32: (a) Timeseries of Elemental Carbon (EC) concentration. **(b)** Timeseries of ratio of EC and OC concentrations at SGP from Jun-Nov 2013.s

Formatted: Caption

430

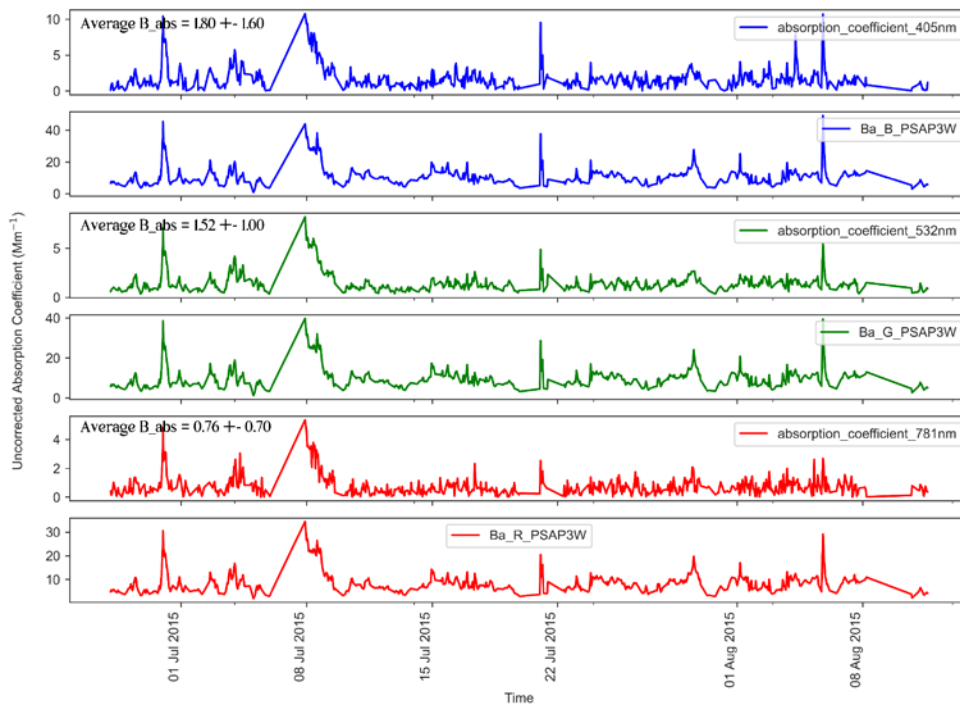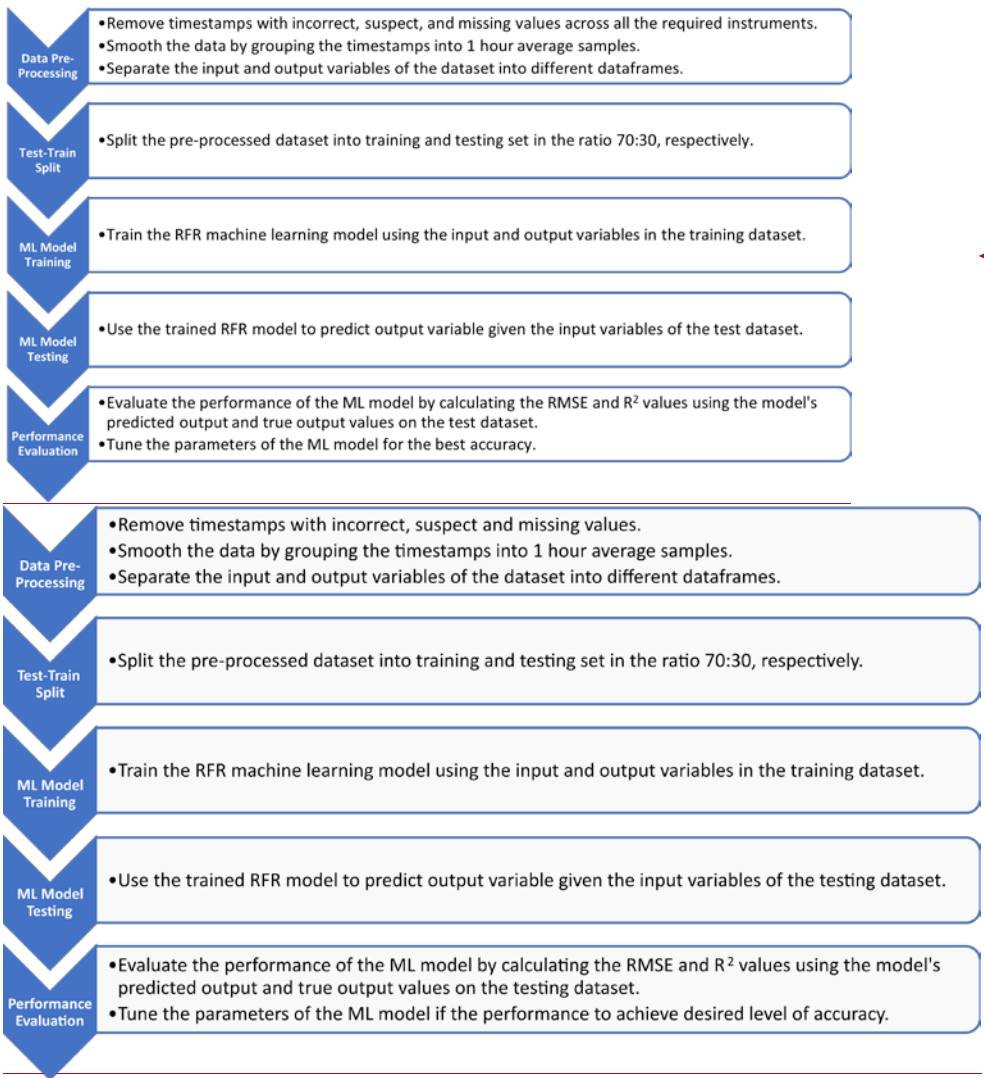**Figure A43:** Timeseries data of uncorrected absorption coefficients as derived from measured by PSAP ($B_{abs\ uncorrected\ PSAP}$) (at 467nm, 530nm and 660nm) and PASS (B_{abs}) (at 405nm, 532nm and 781nm) instrument at the SGP observatory.

Formatted: Font: Italic	
Formatted: Font: Italic, Subscript	
Formatted: Font: Italic	
Formatted: Font: Italic, Subscript	

Data Pre-Processing
- Remove timestamps with incorrect, suspect, and missing values across all the required instruments.
- Smooth the data by grouping the timestamps into 1 hour average samples.
- Separate the input and output variables of the dataset into different dataframes.

Test-Train Split
- Split the pre-processed dataset into training and testing set in the ratio 70:30, respectively.

ML Model Training
- Train the RFR machine learning model using the input and output variables in the training dataset.

ML Model Testing
- Use the trained RFR model to predict output variable given the input variables of the test dataset.

Performance Evaluation
- Evaluate the performance of the ML model by calculating the RMSE and R^2 values using the model's predicted output and true output values on the test dataset.
- Tune the parameters of the ML model for the best accuracy.

Data Pre-Processing
- Remove timestamps with incorrect, suspect and missing values.
- Smooth the data by grouping the timestamps into 1 hour average samples.
- Separate the input and output variables of the dataset into different dataframes.

Test-Train Split
- Split the pre-processed dataset into training and testing set in the ratio 70:30, respectively.

ML Model Training
- Train the RFR machine learning model using the input and output variables in the training dataset.

ML Model Testing
- Use the trained RFR model to predict output variable given the input variables of the testing dataset.

Performance Evaluation
- Evaluate the performance of the ML model by calculating the RMSE and R^2 values using the model's predicted output and true output values on the testing dataset.
- Tune the parameters of the ML model if the performance to achieve desired level of accuracy.

435

Figure A54: Workflow of Machine Learning based correction model developed and used in this study.

440

445

450

Formatted: Normal

455 **Code availability**

https://github.com/joshinkumar/Filter-correction-ML-code.git

Data availability

Atmospheric Radiation Measurement (ARM) user facility. 2009. Photoacoustic Soot Spectrometer (AOSPASS3W). 2015-06-27 to 2015-09-25, Southern Great Plains (SGP) Central Facility, Lamont, OK (C1). Compiled by A. Aiken. ARM Data
460 Center. Data set accessed 2021-12-17 at http://dx.doi.org/10.5439/1190011.

Atmospheric Radiation Measurement (ARM) user facility. 2011. Particle Soot Absorption Photometer (AOSPSAP3W). 2015-06-27 to 2017-09-25, Southern Great Plains (SGP) Central Facility, Lamont, OK (C1). Compiled by A. Koontz and S. Springston. ARM Data Center. Data set accessed 2021-12-17 at http://dx.doi.org/10.5439/1333829.
465

Author contributions. RKC conceived of the study and its design. JK performed the data analysis, developed and implemented the models, and led the preparation of the manuscript. MKD and ACA collected PASS dataset at the SGP site. TP performed the laboratory experiments. RKC, NJS, and PS provided guidance and supervision for carrying out the
490   research tasks, interpretation of results, and contributed to the preparation of the manuscript. All authors were involved in the editing and proofreading of the manuscript.

References

Andrews, E., Sheridan, P., Ogren, J., Hageman, D., Jefferson, A., Wendell, J., Alástuey, A., Alados-Arboledas, L., Bergin, M., and Ealo, M.: Gannet Hallar, A., Hoffer, A., Kalapov, I., Keywood, M., Kim, J., Kim, SW, Kolonjari, F., Labuschagne,
495   C., Lin, NH, Macdonald, A., Mayol-Bracero, OL, McCubbin, IB, Pandolfi, M., Reisen, F., Sharma, S., Sherman, JP, Sorribas, M., and Sun, J.: Overview of the NOAA/ESRL federated aerosol network, B. Am. Meteorol. Soc, 100, 123-135, 2019a.

Andrews, E., Sheridan, P. J., Ogren, J. A., Hageman, D., Jefferson, A., Wendell, J., Alástuey, A., Alados-Arboledas, L., Bergin, M., and Ealo, M.: Overview of the NOAA/ESRL federated aerosol network, Bulletin of the American Meteorological Society, 100, 123-135, 2019b.

Arnott, W. P., Moosmüller, H., Rogers, C. F., Jin, T., and Bruch, R.: Photoacoustic spectrometer for measuring light absorption by aerosol: instrument description, Atmospheric Environment, 33, 2845-2852, 1999.

Biau, G.: Analysis of a random forests model, The Journal of Machine Learning Research, 13, 1063-1095, 2012.

Bond, T. C., Anderson, T. L., and Campbell, D.: Calibration and intercomparison of filter-based measurements of visible light absorption by aerosols, Aerosol Science & Technology, 30, 582-600, 1999.

Breiman, L.: Random forests, Machine learning, 45, 5-32, 2001.

Brown, H., Liu, X., Pokhrel, R., Murphy, S., Lu, Z., Saleh, R., Mielonen, T., Kokkola, H., Bergman, T., and Myhre, G.: Biomass burning aerosols in most climate models are too absorbing, Nature communications, 12, 1-15, 2021.

C Flynn et al., November 2020, DOE/SC-ARM-TR-211, https://www.arm.gov/publications/tech_reports/doe-sc-arm-tr-211.pdf

Chaya Bakshi, Gitconnected, Random Forest Regression, https://levelup.gitconnected.com/random-forest-regression-209c0f354c84

Clarke, A. D.: Integrating sandwich: a new method of measurement of the light absorption coefficient for atmospheric particles, Applied Optics, 21, 3011-3020, 1982.

Collaud Coen, M., Weingartner, E., Apituley, A., Ceburnis, D., Fierz-Schmidhauser, R., Flentje, H., Henzing, J., Jennings, S. G., Moerman, M., and Petzold, A.: Minimizing light absorption measurement artifacts of the Aethalometer: evaluation of five correction algorithms, Atmospheric Measurement Techniques, 3, 457-474, 2010.

Flowers, B., Dubey, M., Mazzoleni, C., Stone, E., Schauer, J., Kim, S.-W., and Yoon, S.: Optical-chemical-microphysical relationships and closure studies for mixed carbonaceous aerosols observed at Jeju Island; 3-laser photoacoustic spectrometer, particle sizing, and filter analysis, Atmospheric chemistry and physics, 10, 10387-10398, 2010.

Gorbunov, B., Hamilton, R., and Hitzenberger, R.: Modeling radiative transfer by aerosol particles on a filter, Aerosol Science & Technology, 36, 123-135, 2002.

Kumar, V., and Sahu, M.: Evaluation of nine machine learning regression algorithms for calibration of low-cost PM2.5 sensor, Journal of Aerosol Science, Volume 157, 2021.

Li, H., McMeeking, G. R., and May, A. A.: Development of a new correction algorithm applicable to any filter-based absorption photometer, Atmospheric Measurement Techniques, 13, 2865-2886, 2020.

Liu, C., Chung, C. E., Yin, Y., and Schnaiter, M.: The absorption Ångström exponent of black carbon: from numerical aspects, Atmospheric Chemistry and Physics, 18, 6259-6273, 2018.

Liu, J., Alexander, L., Fast, J. D., Lindenmaier, R., and Shilling, J. E.: Aerosol characteristics at the Southern Great Plains site during the HI-SCALE campaign, Atmospheric Chemistry and Physics, 21, 5101-5116, 2021.

Müller, T., Virkkula, A., and Ogren, J.: Constrained two-stream algorithm for calculating aerosol light absorption coefficient from the Particle Soot Absorption Photometer, Atmospheric Measurement Techniques, 7, 4049-4070, 2014.

Myers, D. C., Lawler, M. J., Mauldin, R. L., Sjostedt, S., Dubey, M., Abbatt, J., and Smith, J. N.: Indirect Measurements of the Composition of Ultrafine Particles in the Arctic Late-Winter, Journal of Geophysical Research: Atmospheres, 126, e2021JD035428, 2021.

Nakayama, T., Kondo, Y., Moteki, N., Sahu, L., Kinase, T., Kita, K., and Matsumi, Y.: Size-dependent correction factors for absorption measurements using filter-based photometers: PSAP and COSMOS, Journal of Aerosol Science, 41, 333-343, 2010.

26

540   Ogren, J. A.: Comment on "Calibration and intercomparison of filter-based measurements of visible light absorption by aerosols", Aerosol Science and Technology, 44, 589-591, 2010.

Pandey, A., Pervez, S., and Chakrabarty, R. K.: Filter-based measurements of UV–vis mass absorption cross sections of organic carbon aerosol from residential biomass combustion: Preliminary findings and sources of uncertainty, Journal of Quantitative Spectroscopy and Radiative Transfer, 182, 296-304, 2016.

545   Parworth, C., Fast, J., Mei, F., Shippert, T., Sivaraman, C., Tilp, A., Watson, T., and Zhang, Q.: Long-term measurements of submicrometer aerosol chemistry at the Southern Great Plains (SGP) using an Aerosol Chemical Speciation Monitor (ACSM), Atmospheric Environment, 106, 43-55, 2015.

Sheridan, P., Delene, D., and Ogren, J.: Four years of continuous surface aerosol measurements from the Department of Energy's Atmospheric Radiation measurement Program Southern Great Plains Cloud and Radiation Testbed site, Journal of
550   Geophysical Research: Atmospheres, 106, 20735-20747, 2001.

Sherman, J., Sheridan, P., Ogren, J., Andrews, E., Hageman, D., Schmeisser, L., Jefferson, A., and Sharma, S.: A multi-year study of lower tropospheric aerosol variability and systematic relationships from four North American regions, Atmospheric Chemistry and Physics, 15, 12487-12517, 2015.

Shetty, N., Beeler, P., Paik, T., Brechtel, F. J., and Chakrabarty, R. K.: Bias in quantification of light absorption
555   enhancement of black carbon aerosol coated with low-volatility brown carbon, Aerosol Science and Technology, 55, 539-551, 2021.

Shetty, N. J., Pandey, A., Baker, S., Hao, W. M., and Chakrabarty, R. K.: Measuring light absorption by freshly emitted organic aerosols: optical artifacts in traditional solvent-extraction-based methods, Atmospheric Chemistry and Physics, 19, 8817-8830, 2019.

560   Sisterson, D., Peppler, R., Cress, T., Lamb, P., and Turner, D.: The ARM southern great plains (SGP) site, Meteorological Monographs, 57, 6.1-6.14, 2016.

Springston, S.: Particle Soot Absorption Photometer (PSAP) Instrument Handbook, DOE ARM Climate Research Facility, Washington, DC (United States), 2018.

Subramanian, R., Roden, C. A., Boparai, P., and Bond, T. C.: Yellow beads and missing particles: Trouble ahead for filter-
565   based absorption measurements, Aerosol science and technology, 41, 630-637, 2007.

Sumlin, B. J., Heinson, Y. W., Shetty, N., Pandey, A., Pattison, R. S., Baker, S., Hao, W. M., and Chakrabarty, R. K.: UV–Vis–IR spectral complex refractive indices and optical properties of brown carbon aerosol from biomass burning, Journal of Quantitative Spectroscopy and Radiative Transfer, 206, 392-398, 2018.

Uin, J. and Smith, S.: Southern Great Plains (SGP) Aerosol Observing System (AOS) Instrument Handbook, Oak Ridge
570   National Laboratory (ORNL), Oak Ridge, TN (United States …, 2020.

Virkkula, A.: Correction of the calibration of the 3-wavelength Particle Soot Absorption Photometer (3λ PSAP), Aerosol Science and Technology, 44, 706-712, 2010.

Virkkula, A., Ahlquist, N. C., Covert, D. S., Arnott, W. P., Sheridan, P. J., Quinn, P. K., and Coffman, D. J.: Modification, calibration and a field test of an instrument for measuring light absorption by particles, Aerosol Science and Technology, 39,
575   68-83, 2005.

Weingartner, E., Saathoff, H., Schnaiter, M., Streit, N., Bitnar, B., and Baltensperger, U.: Absorption of light by soot particles: determination of the absorption coefficient by means of aethalometers, Journal of Aerosol Science, 34, 1445-1463, 2003.

Zuidema, P., Sedlacek III, A. J., Flynn, C., Springston, S., Delgadillo, R., Zhang, J., Aiken, A. C., Koontz, A., and
580   Muradyan, P.: The Ascension Island boundary layer in the remote southeast Atlantic is often smoky, Geophysical Research Letters, 45, 4456-4465, 2018.